horticulturae

MDPI

Article

CsMYB6 Mediates the Involvement of CsABCG6 in the Transport and Biosynthesis of Anthocyanins in *Chaenomeles speciosa* Flowers Under Drought Conditions

Shuangyu Zhang [1,*], Xiling Chen [2], Xingyue Xue [3], Yaping Xu [3], Xiaoxiao Liu [4] and Aimei Tian [4,*]

[1] The School of Arts and Design, Xi'an University, Xi'an 710065, China
[2] College of Horticulture, Northwest A&F University, Yangling 712100, China; bjyx@nwafu.edu.cn
[3] College of Landscape Architecture and Art, Northwest A&F University, Yangling 712100, China; xuexingyue@nwafu.edu.cn (X.X.); 18574720255@163.com (Y.X.)
[4] School of Biological and Environmental Engineering, Xi'an University, Xi'an 710065, China; xiaoxiaoliulg@163.com
* Correspondence: zhangshuangyu@xawl.edu.cn (S.Z.); tianaimei@126.com (A.T.)

Abstract

Chaenomeles speciosa, a plant species with high ornamental value, exhibited significant darkening of its petal coloration under drought conditions. This chromatic alteration primarily stems from anthocyanin biosynthesis and transport. Through integrated proteomic and transcriptomic analyses, we identified CsABCG6, a transporter of the ABCG subfamily, as a key regulator. The molecular docking analysis preliminarily demonstrated that CsABCG6 bound to anthocyanin monomers. Functional characterization revealed a dual role of CsABCG6 in regard to anthocyanin metabolism; it displayed anthocyanin transport activity in yeast systems, whereas transient transformation assays confirmed its capacity to enhance anthocyanin biosynthesis. Stable transformation experiments in tobacco further validated the anthocyanin-promoting function of the previously identified transcription factor CsMYB6. Yeast one-hybrid (Y1H) and dual-luciferase assays (LUC) established that CsMYB6 transcriptionally activates the CsABCG6 promoter, thus collectively defining the CsMYB6-CsABCG6 signaling module as a critical mechanism for the precise dynamic regulation of anthocyanin metabolism under drought stress.

Keywords: *Chaenomeles speciosa*; CsABCG6; CsMYB6; anthocyanin; drought

Academic Editors: Yue Wu and Changxia Li

Received: 3 October 2025
Revised: 3 November 2025
Accepted: 11 November 2025
Published: 15 November 2025

Citation: Zhang, S.; Chen, X.; Xue, X.; Xu, Y.; Liu, X.; Tian, A. CsMYB6 Mediates the Involvement of CsABCG6 in the Transport and Biosynthesis of Anthocyanins in *Chaenomeles speciosa* Flowers Under Drought Conditions. *Horticulturae* **2025**, *11*, 1378. https://doi.org/10.3390/horticulturae11111378

Copyright: © 2025 by the authors. Licensee MDPI, Basel, Switzerland. This article is an open access article distributed under the terms and conditions of the Creative Commons Attribution (CC BY) license (https://creativecommons.org/licenses/by/4.0/).

1. Introduction

*Chaenomeles specios*a (Sweet) *Nakai*, a shrub belonging to the genus *Chaenomeles* in the family Rosaceae, is valued not only for its brightly colored ornamental flowers but also for its edible and medicinal properties, with its fruit being a commonly used traditional medicine [1]. Previous studies have shown that the petals of *C. speciosa* are rich in anthocyanins, and drought stress has been demonstrated to intensify petal coloration [2,3]. Drought conditions are conducive to the formation of anthocyanins, which are a physiological response of plants to environmental stress and a mechanism of plant self-protection [4]. However, the specific mechanism by which drought influences flower color in *C. speciosa* remains to be fully elucidated.

Droughts can cause a series of physiological reactions in plants, in which hormone regulation is the main physiological activity of plants in response to drought [5]. Several studies have linked drought stress to anthocyanin biosynthesis and transport in various species. For instance, *IbMYC2* regulates anthocyanin accumulation in sweet potatoes under drought conditions [6], while *MsERF17* activates anthocyanin biosynthesis in *Malus spectabilis* (Aiton) *Borkh* leaves under drought stress [7]. In roses, drought stress enhances anthocyanin synthesis and transport in roses, which is mediated by *RcMYB75* and RcGSTFL11 [8]. Droughts promote plant anthocyanin formation in various ways. Synthetic anthocyanins are stored in vacuoles via three transport mechanisms: glutathione S-transferase-mediated transport, membrane transport, and vesicle trafficking [9,10]. Anthocyanins are transported from the cytoplasm to the tonoplasts via the ABC transmembrane transporter [11,12]. Notably, plant ABC transporters are involved in multiple physiological processes through transporting hormones, lipids, metals, and secondary metabolites and are divided into ABCA-ABCG and ABCI subfamilies [13]. Previous studies have shown that the MRP/ABCC subfamily of the ABC transporter family is involved in membrane-mediated transport of anthocyanins. Examples include ZmMRP3 in corn, AtMRP1, AtMRP2, and AtABCC2 in *Arabidopsis thaliana*, OsMRP15 in rice, and VvABCC1 in grapes, which are all considered transporters located on the vacuole membrane responsible for transporting anthocyanins to vacuoles [14–16]; ZmMRP3, ZmMRP5, ZmMRP6, and ZmMRP7 are expressed in all tissues that synthesize anthocyanins [17]. Despite these insights, the regulatory network governing anthocyanin transport under drought conditions is still not well understood.

The ABCG subfamily, the largest among ABC transporters, is involved in the transport of diverse compounds such as terpenoids, alkaloids, lipids, and aromatic volatiles [18,19] and is known to respond to environmental stresses [20]. For example, SlABCG42 in tomato facilitates flavonoid accumulation in roots under drought stress, scavenging ROS, and maintaining membrane integrity [21]. In *Arabidopsis*, AtABCG25 exports ABA from biosynthetic cells, while AtABCG40 imports it into guard cells to induce stomatal closure—a key drought response [22,23]. ABCG17 and ABCG18 have been identified as transporters responsible for ABA transport to the plasma membrane, and their expression is affected under abiotic stress conditions [24]. Nevertheless, the role of ABCG proteins in promoting anthocyanin synthesis and transport under drought remains largely unexplored, and the coordination among relevant factors is still unclear.

MYB transcription factors are key regulators that activate both anthocyanin biosynthesis and transport-related genes [8]. In *Arabidopsis*, overexpression of the MYB75 TF gene AtPAP1 results in significant upregulation of TT19, which is responsible for the transport of cyanidin-3-*O*-glucoside and delphinidin-3-*O*-glucoside [12,25]. Similarly, SbMYB8 and AtPAP1 activate the expression of anthocyanin biosynthesis genes, thereby increasing anthocyanin accumulation and drought resistance [26,27]. Our previous work demonstrated that the CsbZIP24-CsMYB6 module mediates ABA-promoted anthocyanin synthesis in *C. speciosa* under drought [3]. However, how MYB transcription factors coordinate the complete process of anthocyanin accumulation—including both synthesis and transport—is still not fully understood.

In this study, a drought-responsive TF, CsMYB6, and ABCG transport protein, CsABCG6, were identified in *C. speciosa*. CsMYB6 overexpression in *A. thaliana* enhances anthocyanin accumulation. Furthermore, CsABCG6 demonstrated anthocyanin transport functionality in a yeast system, whereas its overexpression promoted anthocyanin accumulation in transgenic *C. speciosa.* We also found that CsMYB6 activates the expression of CsABCG6. These results reveal a molecular mechanism by which CsMYB6 and CsABCG6 collaboratively regulate anthocyanin accumulation under drought stress, providing new insights into the adaptive responses of *C. speciosa*.

2. Methods

2.1. Plant Materials

C. speciosa originated from the south campus of Northwest A & F University in Yangling, China. Flowers of *Chaenomeles speciosa* were transferred to a nutrient solution containing d gradient concentrations of PEG-8000 (0%, 2%, 4%, 6%, 8%, designated as TG0–TG8) to simulate drought stress [2]. Based on physiological indices (anthocyanin content and relative water content), the control (TG0) and moderate drought stress (TG4) groups were selected for proteomics and transcriptomics sequencing (Figure S1) [3]. All samples were immediately frozen in liquid nitrogen and stored at −80 °C until use.

2.2. Subcellular Localization Assay

The cDNA sequence of CsABCG6 was cloned into the pSuper1300-GFP vector. GV3101 *Agrobacterium tumefaciens* cells were transformed with the recombinant plasmid. Bacterial suspensions harboring the construct were infiltrated into *Nicotiana benthamiana* Domin leaves. After 48 h of incubation under low-light conditions, GFP signals were captured using a Leica TCS SP8 laser scanning confocal microscope with excitation at 488 nm and emission at 500–530 nm.

2.3. Molecular Docking Analysis

The tertiary structure of CsABCG6 was modeled using SWISS-MODEL. Ligand-binding pockets were predicted with DEEPSITE (www.playmolecule.com (accessed on 20 July 2023)). Structures of six anthocyanins were retrieved from the TCMSP (https://tcmspe.com/ (21 July 2023)) database and PubChem (https://pubchem.ncbi.nlm.nih.gov/ (21 July 2023)), converted to mol2 format using OpenBabel, and energy-minimized using the MM2 force field in ChemDraw(2022).

2.4. Isolation of Membrane Vesicles from Yeast and Transport Assays

Yeast BY4741 with empty vector pYES2 Ura (pYES2) or pYES2 CsABCG6 was selected as a transformant on a medium lacking uracil [27]. Microsomal vesicles from yeast cells were isolated using published methodologies [28] for in vitro transport experiments. A fluorescence quenching assay with ACMA [29] confirmed vesicle structural integrity. A 1 mL assay mixture containing 2 μM ACMA, 0.4 M glycerol, 5 mM $MgSO_4$, 1 mM DTT, 0.2 M KCl, 25 mM Tris-MES buffer, and 5 mM MgATP was prepared, to which 200 μg of purified vesicles were added. Fluorescence spectroscopy was used to measure fluorescence intensity and obtained an ACMA signal of 485 nm after excitation at 425 nm. The addition of 25 mM ammonium sulfate to the reaction solution assessed proton gradient-dependent ACMA uptake in yeast vesicles.

For anthocyanin transport, rapid filtration techniques were used for uptake experiments [28] and a nitrofiber filter (0.45 mm aperture). 0.2 mL vesicles and cold transport buffers and newly added 1 mM DTT, 6 mM $MgSO_4$, 100 μg/mL creatine kinase, and 10 mM creatine phosphate were mixed for the anthocyanin transport assay. The anthocyanin (1 mM) extracted from the flower petals of *C. speciosa* was determined in 4 mM MgATP and 5 mM GSH with a total reaction volume of 0.8 mL. The filter-bound anthocyanins were dissolved by adding methanol and 0.1% (*v*/*v*) HCl and extracted for 15 min. Then anthocyanin elution was quantified by HPLC [1].

2.5. In Situ Hybridization Assay

CsABCG6 localization was analyzed in TG0 and TG4 floral tissues using Wang et al.'s modified in situ hybridization [30]. Briefly, TG0 and TG4 floral specimens were chemically fixed in RNA-free PFA, dehydrated through an ethanol series, and embedded in

paraffin to generate thin sections (8 μm). After 10 h incubation at 37 °C and xylene deparaffinization, tissues were sequentially processed through ethanol gradients and DEPC-treated water, then subjected to proteinase K digestion (20 μg/mL, 37 °C). DIG-conjugated probes were hybridized overnight at 45 °C, with subsequent washing steps and DAB staining for signal visualization (Nikon Eclipse E100, Nikon Corporation, Tokyo, Japan).

2.6. Transient Expression Assays

To overexpress *CsABCG6* and *CsMYB6*, the ORF of these were cloned into the PC2300 vector to obtain 35S: CsABCG6 and CsMYB6. To suppress *CsABCG6* and *CsMYB6* through virus-induced gene silencing (VIGS), a sequence fragment was cloned into the TRV2 vector.

The methods used for overexpression and suppression of *CsABCG6* and *CsMYB6* by agroinfiltration in *C. speciosa* flowers were described previously [1]. Following vacuum infiltration at −0.08 MPa, petal explants were subjected to three cycles of pressure permeation (2 min per cycle) in the Agrobacterium suspension. Post-infiltration processing included sequential rinses with sterile distilled water and subsequent transfer onto solid growth medium. The samples underwent initial 16 h dark incubation prior to 3–5 days of phenotypic monitoring under controlled culture conditions (25 °C, 16/8 h photoperiod).

2.7. Verification of Stable Transformation of Nicotiana tabacum

CsMYB6 was transformed into GV3101, then collected *Agrobacterium tumefaciens*, activated once with sterile dd H_2O, used 50 mL of sterile dd H_2O suspension (OD600 value is about 0.5), added 5% sucrose and 0.05% Silwet-77, and prepared the infection solution. Tobacco leaves (*Nicotiana tabacum*) underwent 10 min vacuum infiltration with bacterial suspension, then dark-cultured for 24 h to enhance transformation efficiency. After surface sterilization, explants were transferred to antibiotic-containing MS medium and incubated in climate-controlled chambers (25 °C, 60% humidity) under illumination. Following 20–30 days of selection, regenerated seedlings were acclimatized in horticultural containers. Genomic DNA analysis validated heritable transgene integration in surviving lines.

2.8. RT–PCR Validation

Total RNA was isolated using RNA plant plus reagent (Tiangen Biotech, Beijing, China). First-strand cDNA synthesis was performed using the PrimeScript™ Reverse Transcriptase system (Takara Bio, Shiga, Japan) following manufacturer specifications. Quantitative analysis was conducted through real-time PCR (qRT-PCR) with SYBR Green detection. The *Cs18S* gene was used as an internal control. Data analysis followed the $2^{\Delta\Delta Ct}$ method. All experiments included three biological replicates.

2.9. Yeast One-Hybrid Assays (Y1H)

Y1H analysis was conducted by constructing tandem repeats of *CsABCG6* core regulatory elements through multi-fragment ligation into pHIS2 plasmid. Simultaneously, the *CsMYB6* transcriptional sequence was inserted into the pGADT7 expression vector. Following co-transformation of both recombinant plasmids into Y187 yeast competent cells, transformants were initially cultured in selective SD medium lacking leucine and histidine. Subsequent serial dilution spotting was performed on quadruple dropout media (SD/-Ura/-Leu/-His) supplemented with gradient concentrations of 3-amino-1,2,4-triazole (3AT) to assess transcriptional activation capacity through histidine prototrophy restoration.

2.10. Luciferase Reporter Assays (Luc)

For dual-luciferase reporter assays, the *CsABCG6* promoter region was inserted into the multiple cloning site of pGreenII 0800-LUC to create the reporter plasmid, while effector constructs containing *CsMYB6* CDS were engineered in the pGreenII 62-SK expression vector. The recombinant plasmid was introduced into GV3101 via electroporation. Combined bacterial suspensions were pressure-infiltrated into *N. benthamiana* leaves using a needleless syringe. *Agrobacterium*-infiltrated *N. benthamiana* leaves were analyzed using the Dual-Luciferase® Reporter Assay System (Promega). Luminescence was detected with a Berthold Centro XS3 LB 960 microplate reader.

2.11. Statistical Analysis

Physiological data were analyzed by one-way ANOVA using SPSS 25.0 (IBM). Post hoc comparisons were performed using Tukey's test. For qPCR, expression levels were normalized to the internal control *Cs18S*. Anthocyanin content was calibrated against a standard curve and normalized per gram of fresh weight. Bioinformatics processing and graphical visualization were conducted on the omicshare bioinformatics platform. Phylogenetic tree construction was achieved using MEGA 11 molecular evolutionary genetics analysis software. Promoter regulatory elements were identified through cis-acting component prediction via the PlantCARE (https://bioinformatics.psb.ugent.be/webtools/plantcare/html/) web server. Subsequently, TBtools visualization software was employed to generate schematic diagrams of promoter cis-regulatory elements.

3. Result

3.1. Analysis of the Protein Coexpression Network

In order to reveal the proteomic differences in the effects of drought stress on the petals of *C. speciose*, label-free technology was used. The WGCNA (weighted gene co-expression network analysis) algorithm is a typical system biology algorithm for constructing gene co-expression networks, which are used to identify target genes and gene networks. Weighted protein co-expression network analysis (WPCNA) is the application of the WGCNA algorithm in the proteome, and its analysis principle is consistent with that of WGCNA. WPCNA first calculates the Pearson's correlation coefficient between any two proteins. In order to measure whether two proteins have similar expression patterns, it is generally necessary to set a threshold to screen, and the β value is 20 (Figure 1A). A clustering tree was constructed based on the correlation of protein expression, and 15 modules were identified (Figure 1B). The results of module protein clustering are shown in Figure 1C. The correlation heat map between the samples and modules showed that the petal samples under drought conditions were highly correlated with the blue module (Figure 1D). Connectivity values, expression information, and six major database annotations were added to each module protein list obtained by WPCNA. Connectivity refers to the degree of connection between a protein and other proteins (usually only calculated in the module), often called connectivity or degree, or represented by the number k. In general, in a module, the top-ranked proteins in connectivity (k-value) can be considered hub proteins (Table 1). Anthocyanidin synthase (ANS) leads to the synthesis of anthocyanidin pigments. The modules are aggregated into *CsANS* (Unigene0021406). In the blue module, it was found that CsMYB6 (Unigene005811) and CsABCG6 (Unigene0012964) were highly correlated (Table S1).

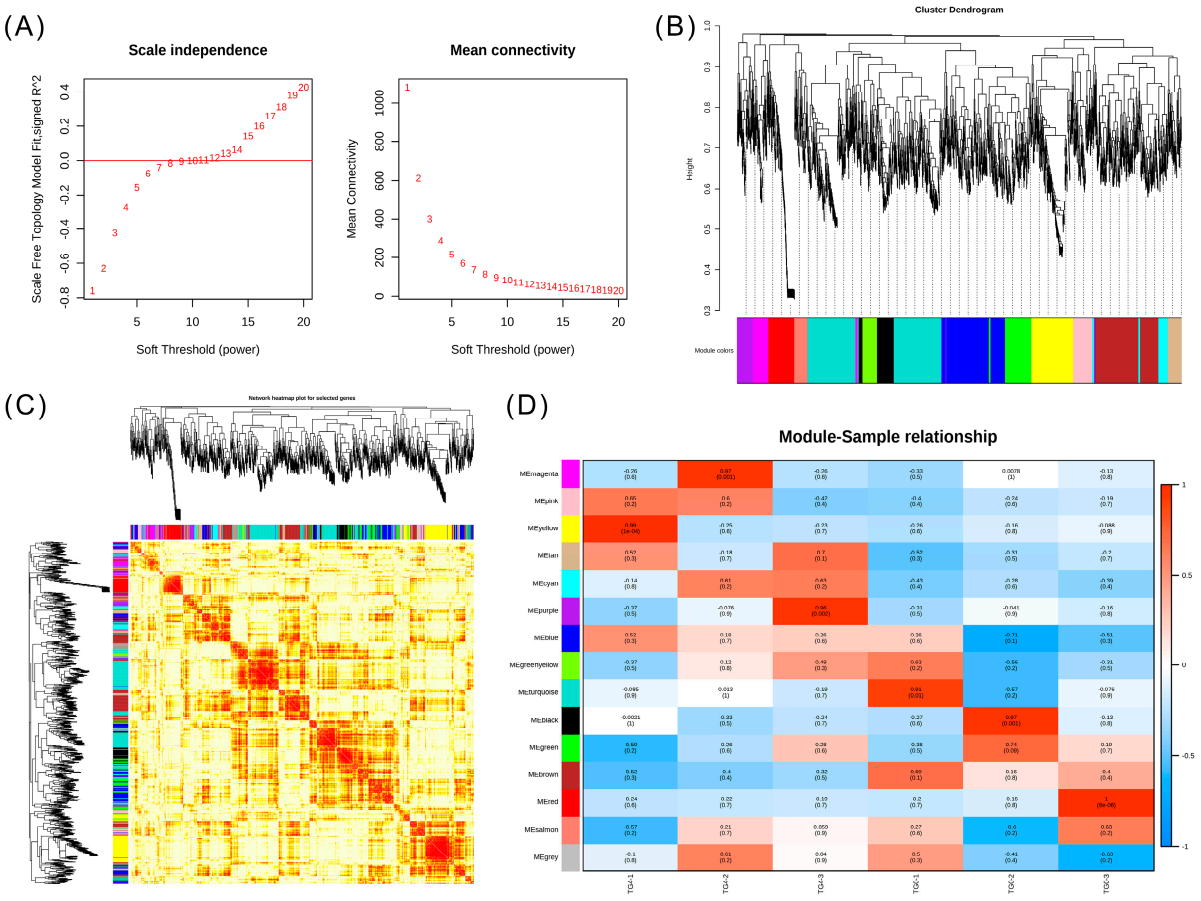

Figure 1. WPCNA in proteome. (**A**) Soft threshold selection graph: the horizontal axis of the graph represents the weight parameter β, that is, the soft threshold. (**B**) Module hierarchical clustering tree diagram: the vertical distance represents the distance between two nodes (between proteins), and the horizontal distance is meaningless. (**C**) Module protein clustering heatmap. (**D**) Correlation heat map between samples and modules.

Table 1. Protein list of each module network node.

Accession	Module Colors	kTotal	kWithin	kOut	kDiff
Unigene0000007	blue	143.84396	69.30067	74.54329	−5.242621
Unigene0000017	turquoise	162.69388	101.32526	61.36862	39.956648
Unigene0000039	purple	52.69120	16.77286	35.91834	−19.145482
Unigene0000046	blue	100.19027	44.25673	55.93355	−11.676821
Unigene0000047	blue	114.65220	79.34737	35.30483	44.042539
Unigene0000048	brown	121.95371	73.66677	48.28695	25.379818
Unigene0000050	yellow	85.64191	14.10864	71.53327	−57.424625
Unigene0000059	blue	158.56537	64.77072	93.79466	−29.023942
Unigene0000063	blue	133.33861	85.81796	47.52065	38.297303
Unigene0000083	blue	100.19525	42.01420	58.18105	−16.166851

3.2. Screening of CsABCG6

Among all of the DAPs and DEGs, we detected five anthocyanin transport synthetic proteins and seven ABCG genes. Of these, CsABCG6 was markedly upregulated in TG4 compared to TG0 (Figure 2A). The secondary structure of the CsABCG6 protein was predicted by the SOPMA online website, and the tertiary structure of the CsABCG6 protein was homologously modeled using SWISS-MODEL. CsABCG6 was used as a template for

homology modeling. Two protein models with GMQE values of 0.79 and 0.46, respectively (Figure 2B). Five protein sequences with high homology to CsABCG6 protein were obtained from the NCBI online website, and then multiple sequence comparison analysis was performed using SnapGene 6.0.2 software. The results are shown in Figure 2. It has an ABC transporter-like (ATP-binding domain) at the C-terminus and an ABC-2 type transporter (transmembrane domain) at the N-terminus (Figure S2). Mega 11 software was used in order to construct a phylogenetic tree of the homologous sequences. A phylogenetic analysis between CsABCG6 and ABCG6 from 38 other plant genes showed that the CsABCG6 protein was highly homologous with MdABCG6-like in apple (*Malus domestica*), followed by PaABCG6-like in European sweet cherry (*Prunus avium*) and PbABCG6-like in white pear (Figure S3). To determine the localization of the CsABCG6 protein in cells, they were constructed into the pCambia1300 vector fused with a GFP fluorescent protein, namely 35S: ABCG6: GFP, and transformed into the leaves of *Nicotiana benthamiana* by Agrobacterium-mediated injection with empty 35S: GFP. DAPI was used for the nuclear staining of tobacco. The results showed that the control group 35S: GFP showed a strong green fluorescence in the whole cells of tobacco leaves, while the green fluorescence of the 35S: ABCG6: GFP fusion vector appeared on the plasma membrane, which did not coincide with DAPI staining. This indicated that the ABCG6 protein was located on the plasma membrane (Figure 2C).

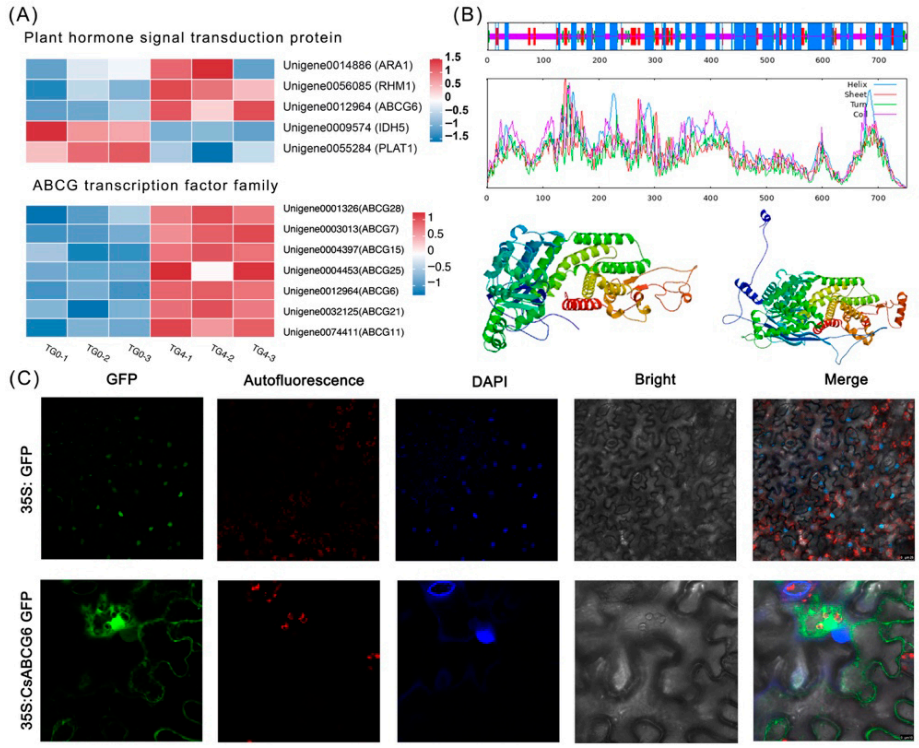

Figure 2. Identification of CsABCG6. (**A**) Differential gene and protein expression heat map. (**B**) Protein structure prediction. A0A5C7GYQ3.1. The protein model numbers were as follows: ABC transporter domain-containing protein; AlphaFold DB model of A0A5C7GYQ3_9ROSI (gene: A0A5C7GYQ3_9ROSI, organism: Acer yangbiense). (**C**) Subcellular localization analysis of CsABCG6.

3.3. Identification of CsABCG6, a Transport Protein from Petals of C. speciosa

To investigate whether CsABCG6 is capable of transporting anthocyanins, we constructed a structural model of the CsABCG6 protein using SWISS-MODEL and performed

molecular docking with six anthocyanins (cyanidin-3-*O*-glucoside, pentahydroxychalcone, cyanidin, eriodictyol, leucocyanidol, and dihydroquercetin). The results showed that CsABCG6 could bind to all six anthocyanins, with the highest binding affinity observed for cyanidin-3-*O*-glucoside (Figure 3A–F, Table 2).

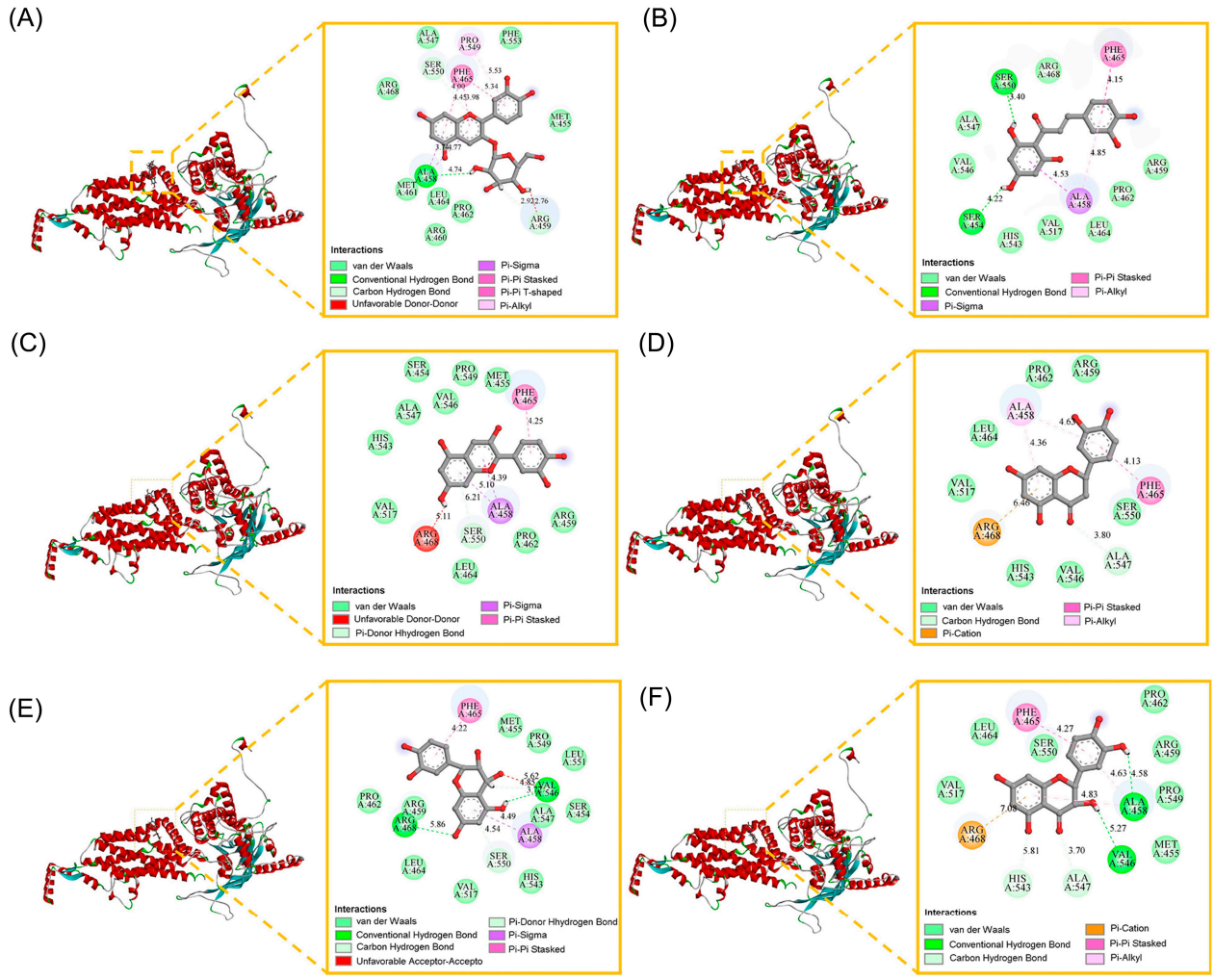

Figure 3. Molecular docking of CsABCG6 with anthocyanin components. (**A**): Cyanidin 3-*O*-glucoside and CsABCG6 (active center: x = 2.11, y = 6.16, z = −9.57). (**B**): 2′, 3, 4, 4′, 6′-Pentahydroxychalcone and CsABCG6 (active center: x = 4.11, y = 6.16, z = −9.57). (**C**): Cyanidin and CsABCG6 (active center: x = 2.11, y = 6.16, z = −9.57). (**D**): Eriodictyol and CsABCG6 (active center: x = 2.11, y = 6.16, z = −9.57). (**E**): Leucocyanidin and CsABCG6 (active center: x = 2.11, y = 6.16, z = −9.57). (**F**): (+)—Dihydroquercetin and CsABCG6 (active center: x = 2.11, y = 6.16, z = −9.57).

Table 2. Summary of PLS regression model R^2 for different numbers of principal components.

	Binding Energy (kcal/mol)					
Active Center (x, y, z)	**Cyanidin 3-O-Glucoside**	**2′, 3, 4, 4′, 6′-Pentahydroxychalcone**	**Cyanidin**	**Eriodictyol**	**leucocianidol**	**(+)-Dihydroquercetin**
2.11, 6.16, −9.57	−7.5	−7.4	−7.2	−7.4	−7.6	−7.5
4.11, 6.16, −9.57	−7.4	−7.6	−7.2	−7.4	−7.5	−7.3
−31.89, −3.84, 2.43	−7.3	−6.7	−6.6	−6.9	−6.7	−6.8

To assess the ability of ABCG6 to transport anthocyanins in heterogeneous expression systems, the ORF encoding CsABCG6 was cloned into the pYES2 plasmid and then

expressed in *Saccharomyces cerevisiae* with defective transporters (BY4741 strain). Yeast cells transformed with the empty vector were used as the control (pYES2) (Figure 4A). Vesicles were isolated from yeast transformants, and we verified their integrity (Figure S3). When compared with the vector control, the yeast cells expressing CsABCG6 had a higher anthocyanin transport capacity (Figure 4B). In addition, the anthocyanin transport capacity increased under drought conditions (Figure 4C-E).

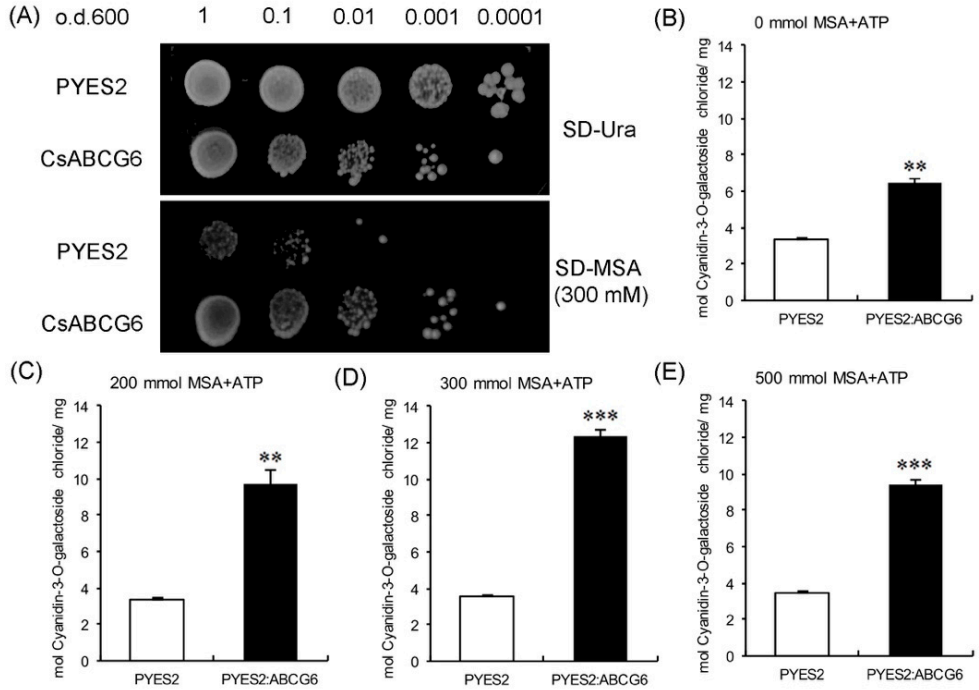

Figure 4. Drought tolerance assay in yeast cells expressing CsABCG6. (**A**): Yeast transformants carrying an empty pYES2 plasmid, ABCG6 (anthocyanins transporter), were cultured on SD-Ura solid medium supplemented with 300 mM mannitol (MSA), and photos were taken after 72 h. (**B–E**): Anthocyanin uptake in yeasts expressing CsABCG6 in the presence of 0–500 mM mannitol (MSA). BY4741 yeast cells were transformed with empty vector pYES2 or with the vector containing CsABCG6 cDNA. The anthocyanin content of the cells was measured with HPLC. The experiment was repeated three times, and the data represent mean ± SD. Asterisks represent the statistical significance between the empty vector and transformants as judged by Student's *t*-test: ** $p < 0.001$, *** $p < 0.0001$.

3.4. CsABCG6 Promotes Anthocyanin Synthesis of C. speciosa

In situ hybridization showed that *CsABCG6* was highly expressed in vascular bundles under drought conditions (Figure 5A). We detected *CsABCG6* expression in *C. speciosa* flowers. Comparing CsABCG6-silenced flowers with the control, it was found that silencing CsABCG6 transcripts hindered the synthesis of anthocyanins, resulting in lighter flower colors than the control under drought conditions (Figure 5B). Concomitantly, we measured the total anthocyanin contents (Figure 5C) and downregulated the anthocyanin-related structural genes and *CsMYB6* (Figure 5D) in *CsABCG6*-silenced flowers. In contrast, the transient overexpression of *CsABCG6* promoted anthocyanin production (Figure 5E), which was supported by a higher total anthocyanin content (Figure 5F), and upregulated the expression of related genes (Figure 5G).

Subsequently, we detected *CsABCG6* expression in *C. speciosa* fruits. *CsABCG6* was briefly overexpressed in fruits, resulting in a noticeable red color around the fruit infiltration site (Figure 6A), which was characterized by an increase in total anthocyanin content when compared to that in the empty control (Figure 6B). Similarly, anthocyanin-related

structural genes (*CHS*, *CHI*, *F3H*, *DRF*, *ANS*, and *UFGT*) and subsequent transcription factors displayed significantly higher transcript levels in fruit peels infiltrated with *CsABCG6* than those in the empty vector control (Figure 6C).

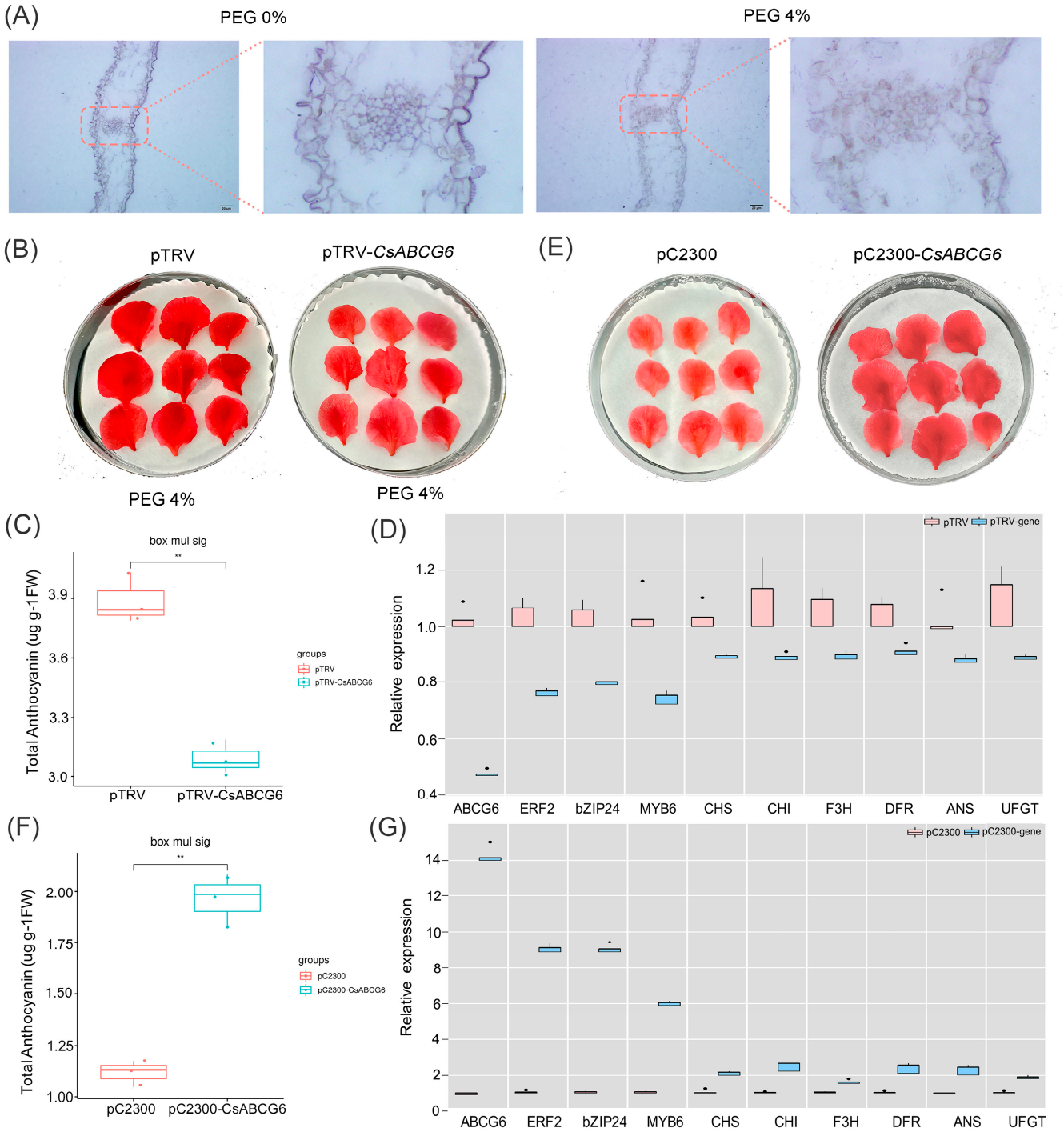

Figure 5. CsABCG6 promoted anthocyanin synthesis in the petals. (**A**): In situ hybridization of CsABCG6. (**B**): Petal phenotype of *C. speciosa* through transient silencing. (**C**): Content of anthocyanins. (**D**): The expression level of *CsABCG6* and the anthocyanin pathway structural gene. (**E**): Petal phenotype of *C. speciosa* through transient overexpression. (**F**): Content of anthocyanins. (**G**): Expression levels of *CsABCG6*, CsMYB6, and anthocyanin pathway structural gene. * $p < 0.05$, ** $p < 0.001$.

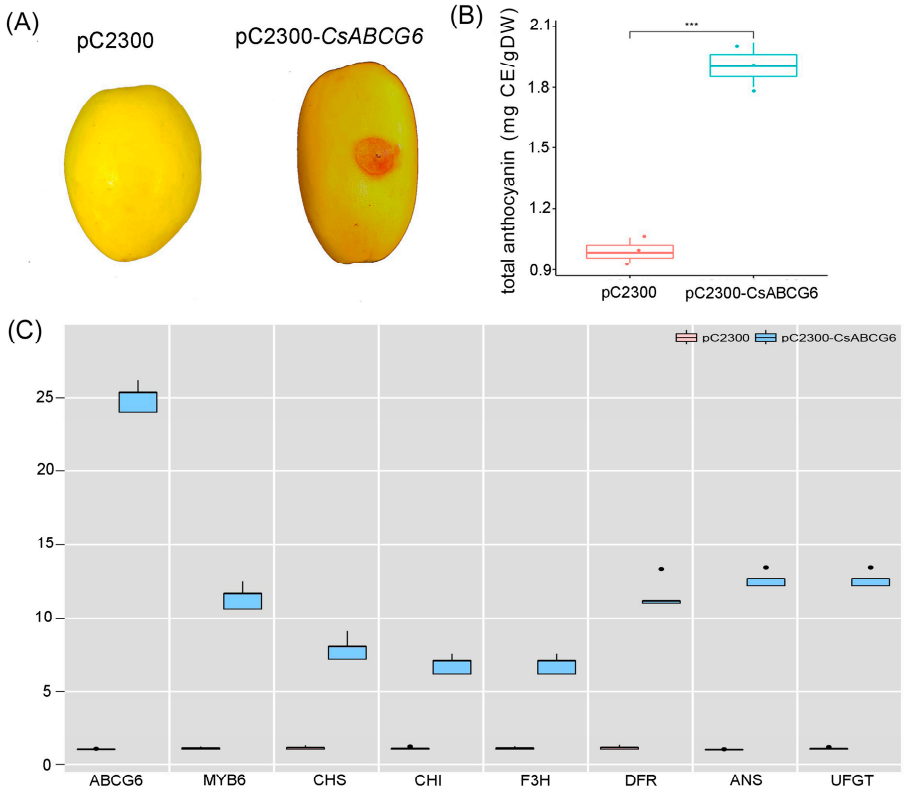

Figure 6. Instantaneous overexpression of *CsABCG6* promotes anthocyanin synthesis in the petal of *C. sinensis*. (**A**): Petal phenotype of *C. sinensis*; (**B**): Content of anthocyanins; (**C**): Expression levels of *CsABCG6* and anthocyanin pathway structural gene. * $p < 0.05$, ***$p < 0.0001$.

3.5. Identification of CsMYB6, *a Transcriptional Activator of Anthocyanin in C. speciosa Flowers*

We have reported that CsMYB6 is a key transcription factor that promotes anthocyanin synthesis. In this study, the function of MYB6 was further verified by its transient expression in the petals of the original *C. speciosa* and its stable expression in exogenous tobacco. We examined the function of CsMYB6 in *C. speciosa* flowers using transient silencing and overexpression. The comparison of *CsMYB6*-silenced flowers with control flowers showed that under drought conditions, silenced CsMYB6 transcripts hindered anthocyanin synthesis, thus resulting in a lighter color than the control flowers (Figure 7A). Concomitantly, we measured the total anthocyanin contents (Figure 7B) and the downregulation of anthocyanin-related structural genes (*CHS*, *CHI*, *F3H*, *DRF*, *ANS*, and *UFGT*) and subsequent transcription factors (ERF2, bZIP24, and MYB6) (Figure 7C) in the CsMYB6-silenced flowers. In contrast, the transient overexpression of CsMYB6 promoted anthocyanin production, which was supported by a higher total anthocyanin content (Figure 7D,E) and upregulated the expression of related genes (Figure 7F). We overexpressed and stably transformed tobacco, which was supported by the upregulated synthesis of anthocyanins and the expression of anthocyanin-related genes in tobacco flowers (Figure 7G–J).

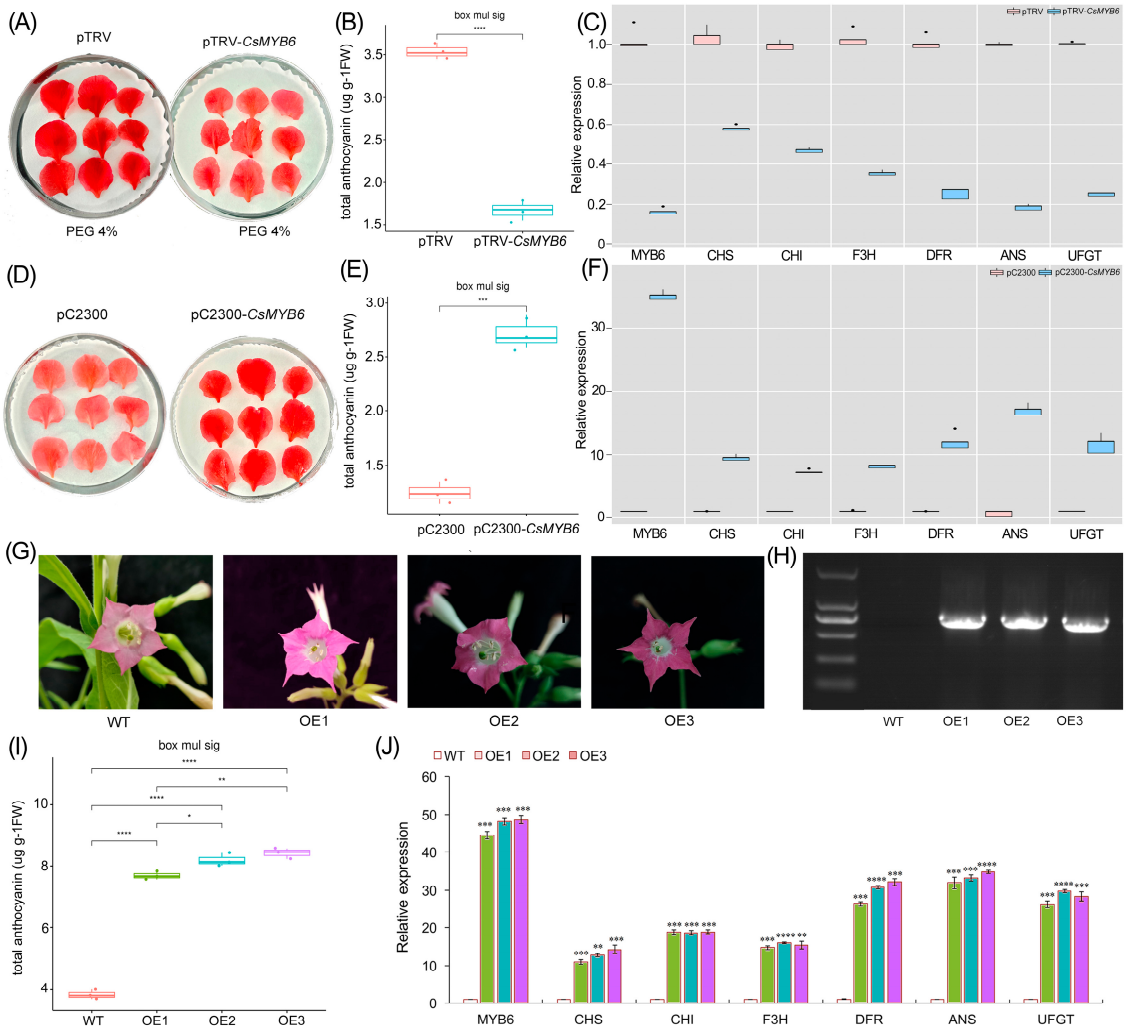

Figure 7. *CsMYB6* promoted anthocyanin synthesis in the petals. (**A**): Petal phenotype of *C. speciosa* through transient silencing. (**B**): Content of anthocyanins. (**C**): The expression level of *CsMYB6* and the anthocyanin pathway structural gene. (**D**): Petal phenotype of *C. speciosa* through transient overexpression. (**E**): Content of anthocyanins. (**F**): Expression levels of CsMYB6 and the anthocyanin pathway structural gene. (**G**): Tobacco petal phenotype. (**H**): Electrophoresis identification. (**I**): Content of anthocyanins. (**J**): The expression levels of CsMYB6 and anthocyanin pathway structural genes. The error line represents the standard deviation of three biological replicates. * $p < 0.05$, ** $p < 0.01$, *** $p < 0.001$, **** $p < 0.0001$.

3.6. CsMYB6 Facilitates the Transcriptional Activity of CsABCG6

To identify the upstream regulatory factor of CsABCG6, we cloned the *CsABCG6* promoter, which yielded 2000 bp fragments. The PlantCARE website was used to predict cis-acting elements in the promoter region of CsABCG6. Analysis of cis-acting elements in the promoter region of *CsABCG6* showed that it contained an MYB binding site involved in drought-inducibility (Figure S5). It has been suggested that CsMYB6 activates expression of CsABCG6 expression by binding to its promoter.

In fact, yeast one-hybrid assays demonstrated specific binding of CsMYB6 to the *CsABCG6* promoter, as evidenced by the robust growth of *pHIS2-CsABCG6* + *pGADT7-CsMYB6* co-transformants on stringent selection medium (-Leu/-His/-Trp) supplemented with 15 mM 3-amino-1,2,4-triazole (3-AT), whereas the control strains (*pHIS2* + *pGADT7-CsMYB6*) exhibited negligible growth (Figure 8A). This interaction suggests a potential regulatory mechanism through which CsABCG6 facilitates CsMYB6-mediated transcriptional activation. To functionally validate this hypothesis, dual-luciferase reporter assays

were conducted using *Nicotiana benthamiana*. The *CsABCG6* promoter (2.1 kb upstream sequence) was fused to firefly luciferase (LUC) in the reporter plasmid, whereas CsMYB6 served as an effector in the pGreenII 62-SK system. *Agrobacterium tumefaciens* GV3101 strains harboring these constructs were co-infiltrated into the tobacco leaves. Quantification of luminescence revealed an increase in LUC activity when *CsMYB6* was co-expressed with the *CsABCG6* promoter compared to empty vector controls (Figure 8B,C). These results confirmed that CsMYB6 directly activates *CsABCG6* transcription through promoter binding, establishing a positive feedback regulatory loop.

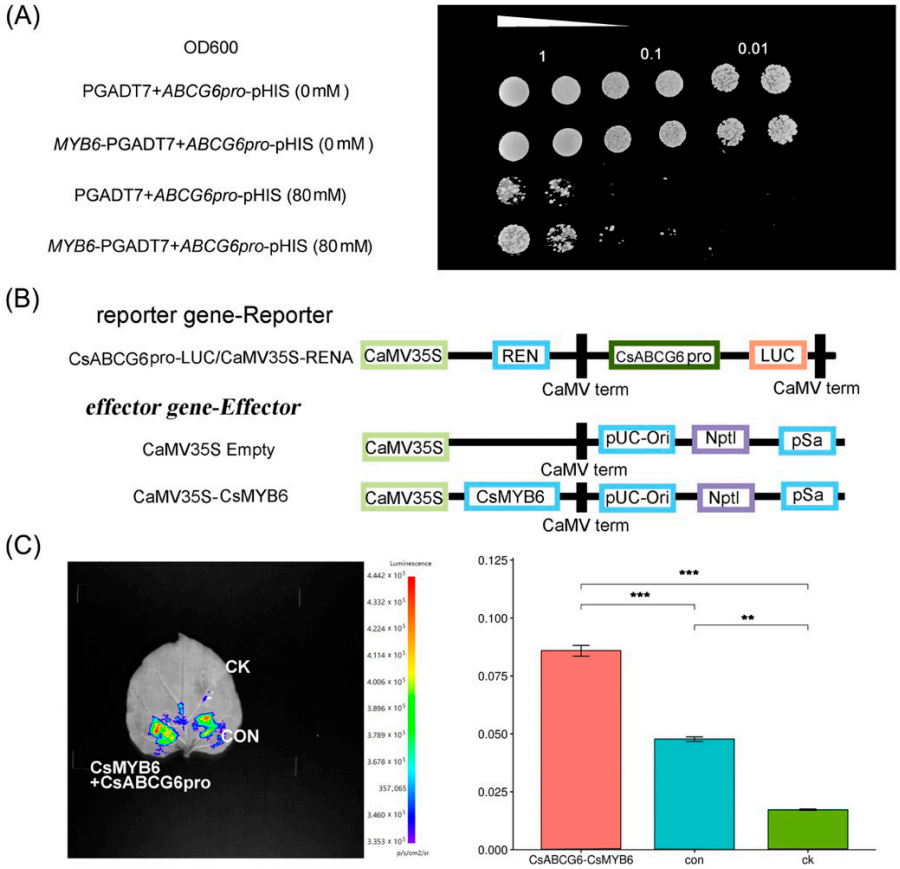

Figure 8. CsABCG6 facilitates the transcriptional activity of CsMYB6. (**A**): Interaction of CsMYB6 with CsABCG6 elements evaluated by yeast one-hybrid assays: ABCG6/His control; (**B**): Schematic representations of the effector vectors CsMYB6 and the firefly luciferase reporter vectors containing the CsABCG6 promoters. (**C**): The dual luciferase assays in tobacco leaves showing that CsMYB6 activates CsABCG6 promoters. The promoter fragment of CsABCG6 was cloned into the pGreenII 0800-LUC vector to generate the reporter constructs. The effectors were generated by recombining the CsMYB6 genes into the pGreenII 62-SK vector. The representative pictures were taken. LUC/REN activity detection to verify CsMYB6 to activate the CsABCG6 promoter. An empty vector was used as the reference. Asterisks denote *T*-test significance: ** $p < 0.01$ and *** $p < 0.001$.

4. Discussion

4.1. Identification of CsABCG6, a Transport Protein from Petals of C. speciosa

C. speciosa is widely used as an ornamental plant. Abiotic stress alters the chemical characteristics and also the quantity of plant compounds. Previous studies have demonstrated that the anthocyanin synthesis deepens the flower color of *C. speciosa* under drought conditions. Metabolomics and transcriptomics are applied to abiotic stress identification of differential metabolites and differential genes [31,32]. In this study, label-free

proteomics was used in order to screen proteins that affect the flower color change in *C. speciosa* under drought conditions.

In this study, we identified CsABCG6, a plasma membrane-localized transporter, through label-free proteomic screening of *C. speciosa* petals under drought stress. ABCG-related genes were screened in the transcriptome of previous studies, and ABCG6 was found to be highly expressed in petals with high anthocyanin content. While ABCC/MRP-type transporters, such as ZmMRP3 and VvABCC1, are well-established in anthocyanin vacuolar sequestration [33,34], the role of ABCG subfamily members remains less explored. A notable exception is AtABCG26, which facilitates anthocyanin efflux to the apoplast in *Arabidopsis* [34]. Our molecular docking analysis indicated strong binding affinity between CsABCG6 and cyanidin-3-*O*-galactoside. Subcellular localization results showed that CsABCG6 was localized to the plasma membrane. In situ hybridization also showed that ABCG6 was highly expressed in the cytoplasm. Our results demonstrate that ABCG6 transports anthocyanins in yeast. In summary, this study combined molecular docking, yeast function verification, and expression localization analysis to confirm that CsABCG6 can transport anthocyanins and expanded the functional understanding of the ABCG subfamily in anthocyanin metabolism.

4.2. CsABCG6 Mediates Drought to Regulate Anthocyanin Biosynthesis

ABCG is involved in stress responses such as drought stress, which improves plant resistance to abiotic stresses [35]. MsABCG1 from *Medicago sativa* L. responds significantly to drought stress [36]. PrABCG15 from *Pyrus* L. is mainly involved in flavonoid transport [37]. Beyond its transport function, CsABCG6 contributes to enhanced anthocyanin accumulation under drought. CsABCG6 not only shows the ability to transport anthocyanin precursors across the membrane, but it also promotes anthocyanin synthesis. Beyond a conventional transport role, our findings indicate that CsABCG6 contributes to elevated anthocyanin accumulation under drought conditions. Transient overexpression of CsABCG6 significantly increased anthocyanin content, whereas its silencing via VIGS led to a marked reduction, confirming its essential role in drought-induced pigmentation.

A key question is the mechanistic basis for CsABCG6's dual role in both transport and biosynthesis enhancement. We propose two non-exclusive explanations: First, the enhancement of anthocyanin biosynthesis is likely indirect, mediated through transcriptional crosstalk. Subsequently, we observed coordinated upregulation of anthocyanin structural genes (*CHS*, *CHI*, *F3H*, *DFR*, *ANS*, *UFGT*) and the key regulatory transcription factor CsMYB6 (Figures 5G and 6C). This suggests that CsABCG6's activity may establish a feed-forward loop, potentially facilitated by the transport of anthocyanins or their precursors, which could in turn amplify the expression of biosynthetic genes via the CsMYB6 transcription factor.

Second, a direct feedback mechanism via altered metabolite flux could also contribute. Efficient transport of anthocyanin precursors by CsABCG6 might reduce end-product inhibition in the biosynthetic pathway, thereby accelerating flux through the pathway. While our current data does not directly measure substrate flux or feedback inhibition, this remains a plausible auxiliary mechanism. The transcriptional coordination is further reinforced by the finding that CsMYB6 directly binds to the CsABCG6 promoter and activates its expression, as shown by Y1H and dual-luciferase assays. Thus, unlike the classic MBW complex that primarily activates biosynthetic genes, the CsMYB6-CsABCG6 module represents a cohesive "synthesis-and-transport" regulon. In this model, CsMYB6 concurrently activates biosynthetic genes (e.g., *CsUFGT*, *CsANS*) and the transporter CsABCG6, enabling synchronized synthesis and membrane transport (Figure 9).

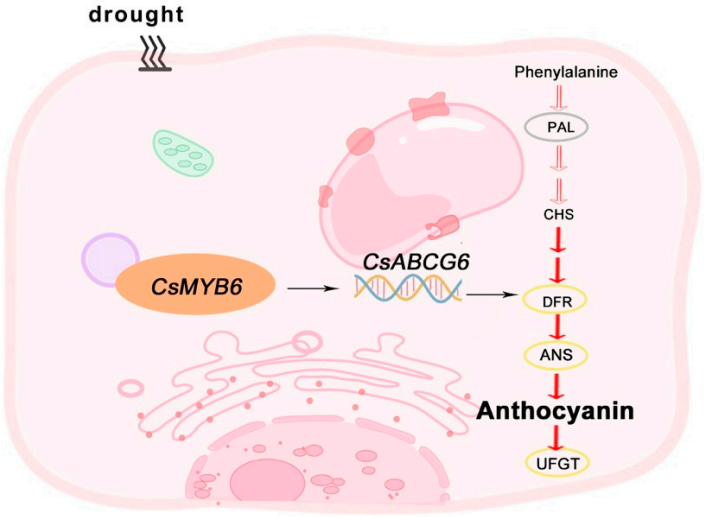

Figure 9. CsMYB6-CsABCG6 mediated anthocyanin biosynthesis working model in response to drought stress.

In summary, CsABCG6 promotes anthocyanin accumulation through a composite mechanism: it directly facilitates anthocyanin (or precursor) transport while indirectly boosting biosynthesis via transcriptional upregulation, primarily mediated by CsMYB6. This "transport-and-transcript" coordinated model underscores a sophisticated level of regulation in plant secondary metabolism, expanding the functional paradigm for ABC transporters beyond mere metabolite transport.

5. Conclusions

In this study, the molecular mechanism of petal color deepening of *Chaenomeles speciosa* under drought stress was revealed by integrated proteomics and transcriptome analysis. We identified a key transporter, CsABCG6, which not only directly binds to and transports anthocyanins but also exhibits a dual function of promoting anthocyanin synthesis in plants. Further study found that the transcription factor CsMYB6 can directly bind and transcriptionally activate the promoter of *CsABCG6*. These pieces of evidence together elucidate a regulatory pathway composed of the CsMYB6-*CsABCG6* module: under drought stress, CsMYB6 enhances the transport capacity of anthocyanins by up-regulating the expression of *CsABCG6*. On the other hand, it indirectly or directly promotes the biosynthesis of anthocyanins, eventually leading to the accumulation of anthocyanins and deepening of color in petals. This study is the first to analyze this key signaling pathway that accurately regulates anthocyanin metabolism in response to drought stress in *C. speciosa*, which not only provides a new theoretical basis for understanding the mechanism of flower color formation under abiotic stress but also plays an important molecular foundation for the subsequent cultivation of stress-resistant ornamental plants through genetic improvement.

Supplementary Materials: The following supporting information can be downloaded at https://www.mdpi.com/article/10.3390/horticulturae11111378/s1: Figure S1: Petal color changes of C. speciosa treated with different PEG concentrations; Figure S2: CsABCG6 protein bioinformatics analysis; Figure S3: CsABCG6 protein physicochemical properties analysis; Figure S4: Verification of the integrity of empty yeast vesicles for PYES2; Figure S5: Analysis of cis-acting elements in CsABCG6 promoter region; Table S1: A list of overlapping DAPs leading to CsABCG6 selection.

Author Contributions: Conceptualization, S.Z., A.T.; methodology, S.Z.; software, X.X.; validation, S.Z., X.L.; investigation, S.Z., X.L.; resources, S.Z., A.T.; data curation, X.C., Y.X.; writing—original draft preparation, S.Z.; writing—review and editing, A.T.; visualization, S.Z., X.L. All authors have read and agreed to the published version of the manuscript.

Funding: This research was funded by Xi 'an Academy of Social Sciences General Project [grant number 25ZL26 and 25ZL53], Key Core Technology R&D Projects of Shaanxi Province [grant number 2025NC-YBXM-072], General special scientific research project in Shaanxi Provincial Department of Education [grant number 24JK0625], National Natural Science Foundation of China [grant number 32402615] .

Data Availability Statement: The original contributions presented in this study are included in the article/supplementary material. Further inquiries can be directed to the corresponding author(s).

Conflicts of Interest: The authors declare no conflicts of interest.

References

1. Bi, H.T.; Guo, M.L.; Wang, J.W.; Qu, Y.; Du, W.L.; Zhang, K.M. Transcriptome analysis reveals anthocyanin acts as a protectant in Begonia semperflorens under low temperature. *ACTA Physiol. Plant.* **2017**, *40*, 968. https://doi.org/10.1007/s11738-017-2578-3.
2. Zhang, S.; Ren, Y.; Zhao, Q.; Wu, Y.; Zhuo, Y.; Li, H. Drought-induced CsMYB6 interacts with CsbHLH111 to regulate anthocyanin biosynthesis in *Chaenomeles speciosa*. *Physiol. Plant.* **2023**, *175*, e13859. https://doi.org/10.1111/PPL.13859.
3. Zhang, S.; Chen, X.; Ren, Y.; Xue, X.; Xu, Y.; Wang, Q.; Xie, Y.; Zhang, T.; Lin, J.; Chen, X.; et al. Multi-omics analysis reveals anthocyanin synthesis is associated with drought stress tolerance in *Chaenomeles speciosa flowers*. *J. Clean. Prod.* **2024**, *476*, 143755. https://doi.org/10.1016/J.JCLEPRO.2024.143755.
4. Jaleel, C.A.; Manivannan, P.; Wahid, A.; Farooq, M.; Al-Juburi, H.J.; Somasundaram, R.; Panneerselvam, R. Melatonin alleviates drought stress and increases lutein and zeaxanthin industrial pigments in African marigold by some physiological regulations. *Ind. C. & P.* **2024**, 222, 120089.
5. Pustovoitova, N.T.; Zhdanova, E.N.; Zholkevich, N.V. Changes in the levels of IAA and ABA in cucumber leaves under progressive soil drought. *Russ. J. Plant Physiol.* **2004**, *51*, 513–517. https://doi.org/10.1023/B:RUPP.0000035745.82509.bc.
6. Hu, Y.; Zhao, H.; Xue, L.; Nie, N.; Zhang, H.; Zhao, N.; He, S.; Liu, Q.; Gao, S.; Zhai, H. IbMYC2 contributes to salt and drought stress tolerance via modulating anthocyanin accumulation and ROS-scavenging system in sweet potato. *Int. J. Mol. Sci.* **2024**, *25*, 2096. https://doi.org/10.3390/IJMS25042096.
7. Xu, Y.; Liu, Y.; Yue, L.; Zhang, S.; Wei, J.; Zhang, Y.; Huang, Y.; Zhao, R.; Zou, W.; Feng, H.; et al. MsERF17 promotes ethylene-induced anthocyanin biosynthesis under drought conditions in *Malus spectabilis* leaves. *Plant Cell Environ.* **2024**, *48*, 1890–1902. https://doi.org/10.1111/PCE.15271.
8. Ma, M.; Li, R.; Li, Y.; Dai, W.; Shang, J.; He, Y.; Xiang, F.; Yang, Y.; Wang, J.; Huang, Z.; et al. Anthocyanin biosynthesis and transport synergistically modulated by RcMYB75 and RcGSTFL11 play a pivotal role in the feedforward loop in response to drought stress. *Plant J.* **2025**, *121*, e17240. https://doi.org/10.1111/TPJ.17240.
9. Zhao, J.; Dixon, R.A. MATE transporters facilitate vacuolar uptake of epicatechin 3′-O-glucoside for proanthocyanidin biosynthesis in *Medicago truncatula* and *Arabidopsis*. *Plant Cell* **2009**, *21*, 2323–2340. https://doi.org/10.1105/tpc.109.067819.
10. Gomez, C.; Conejero, G.; Torregrosa, L.; Cheynier, V.; Terrier, N.; Ageorges, A. In vivo grapevine anthocyanin transport involves vesicle-mediated trafficking and the contribution of anthoMATE transporters and GST. *Plant J.* **2011**, *67*, 960–970. https://doi.org/10.1111/J.1365-313X.2011.04648.X.
11. Marrs, K.A.; Alfenito, M.R.; Lloyd, A.M.; Walbot, V. A glutathione S-transferase involved in vacuolar transfer encoded by the maize gene Bronze-2. *Nature* **1995**, *375*, 397–400. https://doi.org/10.1038/375397a0.
12. Sun, Y.; Li, H.; Huang, J. *Arabidopsis* TT19 functions as a carrier to transport anthocyanin from the cytosol to tonoplasts. *Mol. Plant* **2012**, *5*, 387–400. https://doi.org/10.1093/mp/ssr110.
13. Hwang, J.U.; Song, W.Y.; Hong, D.; Ko, D.; Yamaoka, Y.; Jang, S.; Yim, S.; Lee, E.; Khare, D.; Kim, K.; et al. Plant ABC transporters enable many unique aspects of a terrestrial plant's lifestyle. *Mol. Plant* **2016**, *9*, 338–355. https://doi.org/10.1016/j.molp.2016.02.003.
14. Liu, G.; Sánchez-Fernández, R.; Li, Z.S.; Rea, P.A. Enhanced multispecificity of arabidopsis vacuolar multidrug resistance-associated protein-type ATP-binding cassette transporter, AtMRP2. *J. Biol. Chem.* **2001**, *276*, 8648–8656.

15. Burla, B.; Pfrunder, S.; Nagy, R.; Francisco, R.M.; Lee, Y.; Martinoiaet, E. Vacuolar transport of abscisic acid glucosyl ester is mediated by ATP-binding cassette and proton-antiport mechanisms in Arabidopsis. *Plant Physiol.* **2013**, *163*, 1446–1458. https://doi.org/10.1104/pp.113.222547.
16. Behrens, C.E.; Smith, K.E.; Iancu, C.V.; Choe, J.-Y.; Dean, J.V. Transport of anthocyanins and other flavonoids by the Arabidopsis ATP-Binding cassette transporter AtABCC2. *Sci. Rep.* **2019**, *9*, 437. https://doi.org/10.1038/s41598-018-37504-8.
17. Zhu, Q.; Xie, X.; Zhang, J.; Xiang, G.; Li, Y.; Wu, H. In silico analysis of a MRP transporter gene reveals its possibe role in anthocyanins or flavonoids transport in *Oryze sativa*. *Am. J. Plant Sci.* **2013**, *4*, 555–560. https://doi.org/10.4236/ajps.2013.43072.
18. Biała, W.; Banasiak, J.; Jarzyniak, K.; Pawela, A.; Jasiński, M. Medicago truncatula ABCG10 is a transporter of 4-coumarate and liquiritigenin in the medicarpin biosynthetic pathway. *J. Exp. Bot.* **2017**, *68*, 3231–3241. https://doi.org/10.1093/jxb/erx059.
19. Zhang, D.; Yu, Z.; Zeng, B.; Liu, X. Genome-wide analysis of the ABC gene family in almond and functional predictions during flower development, freezing stress, and salt stress. *BMC Plant Biol.* **2024**, *24*, 12. https://doi.org/10.1186/S12870-023-04698-7.
20. Gräfe, K.; Schmitt, L. The ABC transporter G subfamily in *Arabidopsis thaliana*. *J. Exp. Bot.* **2021**, *72*, 92–106. https://doi.org/10.1093/jxb/eraa260.
21. Annadurai, K.M.; Senthil, A.; Kuppusamy, A.; Maduraimuthu, D.; Karuppasami, K.; Ramakrishnan, S.; Subramanian, M.; Sampathrajan, V.; Selvaraju, K. Melatonin imparts tolerance to combined drought and high-temperature stresses in tomato through osmotic adjustment and ABA accumulation. *Front. Plant Sci.* **2024**, *15*, 1382914. https://doi.org/10.3389/FPLS.2024.1382914.
22. Kuromori, T.; Miyaji, T.; Yabuuchi, H.; Shimizu, H.; Sugimoto, E.; Kamiya, A.; Moriyama, Y.; Shinozakiet, K. ABC transporter AtABCG25 is involved in abscisic acid transport and responses. *Proc. Natl. Acad. Sci. USA* **2010**, *107*, 2361–2366. https://doi.org/10.1073/pnas.0912516107.
23. Kang, J.; Hwang, J.-U.; Lee, M.; Kim, Y.-Y.; Assmann, S.M.; Martinoia, E.; Lee, Y. PDR-type ABC transporter mediates cellular uptake of the phytohormone abscisic acid. *Plant Cell* **2015**, *27*, 1262–1279. https://doi.org/10.1073/pnas.0909222107.
24. Zhang, Y.; Kilambi, H.; Liu, J.; Bar, H.; Lazary, S.; Egbaria, A.; Ripper, D.; Charrier, L.; Belew, Z.M.; Wulff, N.; et al. ABA homeostasis and long-distance translocation are redundantly regulated by ABCG ABA importers. *Sci. Adv.* **2021**, *7*, eabf6069. https://doi.org/10.1126/SCIADV.ABF6069.
25. Cui, Y.; Fan, J.; Lu, C.; Ren, J.; Qi, F.; Huang, H.; Dai, S. ScGST3 and multiple R2R3-MYB transcription factors function in anthocyanin accumulation in *Senecio cruentus*. *Plant Sci.* **2021**, *313*, 111094. https://doi.org/10.1016/J.PLANTSCI.2021.111094.
26. Sun, X.; Wang, F.; Cai, H.; Zhao, Y.; Ji, W.; Zhu, Y. Functional characterization of an *Arabidopsis* prolyl aminopeptidase AtPAP1 in response to salt and drought stresses. *Plant Cell* **2013**, *114*, 325–338. https://doi.org/10.1007/s11240-013-0328-9.
27. Yuan, Y.; Qi, L.; Yang, J.; Wu, C.; Liu, Y.; Huang, Q. A *Scutellaria baicalensis* R2R3-MYB gene, SbMYB8, regulates flavonoid biosynthesis and improves drought stress tolerance in transgenic tobacco. *Plant Cell* **2015**, *120*, 961–997. https://doi.org/10.1007/s11240-014-0650-x.
28. Ashraf, M.A.; Akihiro, T.; Ito, K.; Kumagai, S.; Sugita, R.; Tanoi, K.; Rahmanet, A. ATP binding cassette proteins ABCG37 and ABCG33 function as potassium-independent cesium uptake carriers in Arabidopsis roots. *Mol. Plant* **2021**, *14*, 664–678. https://doi.org/10.1016/J.MOLP.2021.02.002.
29. Sarah, C.B.; Samir, B.; John, L.R.; Voula, K. Structure of a dimeric full-length ABC transporter. *Nat. Commun.* **2024**, *1*, 9946. https://doi.org/10.1038/S41467-024-54147-8.
30. Gomez, C.; Terrier, N.; Torregrosa, L.; Vialet, S.; Fournier-Level, A.; Verriès, C.; Souquet, J.-M.; Mazauric, J.-P.; Klein, M.; Cheynier, V.; et al. Grapevine MATE-type proteins act as vacuolar H+-dependent acylated anthocyanin transporters. *Plant Physiol.* **2009**, *150*, 402–415. https://doi.org/10.1104/pp.109.135624.
31. Wang, P.; Liao, H.; Zhang, W.; Yu, X.; Zhang, R.; Shan, H.; Duan, X.; Yao, X.; Kong, X. Flexibility in the structure of spiral flowers and its underlying mechanisms. *Nat. Plants* **2015**, *2*, 15188. https://doi.org/10.1038/nplants.2015.188.
32. Hammou, A.; El Caid, B.; Harrouni, C.; Daoud, S. Germination enhancement, antioxidant enzyme activity, and metabolite changes in late *Argania spinosa* kernels under salinity. *J. Arid Environ.* **2023**, *219*, 105095. https://doi.org/10.1016/j.jaridenv.2023.105095.
33. Goodman, C.D.; Casati, P.; Walbot, V. A multidrug resistance–associated protein involved in anthocyanin transport in Zea mays. *Plant Cell* **2004**, *16*, 1812–1826. https://doi.org/10.1105/tpc.022574.
34. Francisco, R.M.; Regalado, A.; Ageorges, A.; Burla, B.J.; Bassin, B.; Eisenach, C.; Zarrouk, O.; Vialet, S.; Marlin, T.; Chaves, M.M.; et al. ABCC1, an ATP binding cassette protein from grape berry, transports anthocyanidin 3-O-glucosides. *Plant Cell* **2013**, *25*, 1840–1854. https://doi.org/10.1105/tpc.112.102152.
35. Kuromori, T.; Sugimoto, E.; Shinozaki, K. Arabidopsis mutants of AtABCG22, an ABC transporter gene, increase water transpiration and drought susceptibility. *Plant J.* **2011**, *67*, 885–894. https://doi.org/10.1111/J.1365-313X.2011.04641.X.

36. Yang, R.; Yang, Y.; Yuan, Y.; Zhang, B.; Liu, T.; Shao, Z.; Li, Y.; Yang, P.; An, J.; Cao, Y. MsABCG1, ATP-binding cassette G transporter from Medicago sativa, improves drought tolerance in transgenic *Nicotiana tabacum*. *Physiol. Plant.* **2024**, *176*, e14392. https://doi.org/10.1111/PPL.14446.
37. Zhang, S.; Xu, J.; Zhang, Y.; Cao, Y. Identification and characterization of ABCG15—A gene required for exocarp color differentiation in pear. *Genes* **2023**, *14*, 1827. https://doi.org/10.3390/GENES14091827.

Disclaimer/Publisher's Note: The statements, opinions and data contained in all publications are solely those of the individual author(s) and contributor(s) and not of MDPI and/or the editor(s). MDPI and/or the editor(s) disclaim responsibility for any injury to people or property resulting from any ideas, methods, instructions or products referred to in the content.